

# A hot, nebular-dominated galaxy interacting with a pristine PopIII system uncovered by JWST

Henriette Reumert<sup>1,2</sup>, Kasper E. Heintz<sup>3,1,2</sup>, Clara L. Pollock<sup>1,2</sup>, Alex J. Cameron<sup>1,2</sup>, Gabriel B. Brammer<sup>1,2</sup>, Harley Katz<sup>4,5</sup>, Albert Sneppen<sup>1,2</sup>, Joris Witstok<sup>1,2</sup>, Chamilla Terp<sup>1,2</sup>, and Darach Watson<sup>1,2</sup>

<sup>1</sup> Cosmic Dawn Center (DAWN), Denmark; e-mail: henriette.reumert@nbi.ku.dk

<sup>2</sup> Niels Bohr Institute, University of Copenhagen, Jagtvej 128, 2200 Copenhagen N, Denmark

<sup>3</sup> DTU Space, Technical University of Denmark, Elektrovej 327, DK2800 Kgs. Lyngby, Denmark

<sup>4</sup> Department of Astronomy & Astrophysics, University of Chicago, 5640 S Ellis Avenue, Chicago, IL 60637, USA

<sup>5</sup> Kavli Institute for Cosmological Physics, University of Chicago, Chicago IL 60637, USA

Received March 17, 2026

## ABSTRACT

The discovery of galaxies with extremely strong nebular continuum emission at high redshifts provide novel, unique insights into the conditions under which the first super-massive stars formed. Here we identify a galaxy at redshift  $z = 5.124$  observed by the *JWST* CAPERS survey that exhibits a prominent turnover in the rest-frame UV continuum and a pronounced Balmer ‘jump’. We model the entire *JWST*/NIRSpec Prism spectrum from rest-frame UV to optical wavelength, finding that a dominant ( $> 95\%$ ) nebular continuum emission can accurately reproduce the spectral shape across all wavelengths. We tested an alternative model with strong damped Ly $\alpha$  absorption (DLA), but found that it is not able to match the shape of the turnover without invoking a large freedom in the redshift of the absorber. The nebular continuum emission model reveals a hot ( $T = (5.3 \pm 0.2) \times 10^4$  K) and dense ( $n_e = (5.4 \pm 0.8) \times 10^3$  cm<sup>-3</sup>) nebular region powering the origin of the spectral shape. We also note the presence of a ‘blue’ companion source at the same redshift, offset by 3 kpc to the main galaxy. Intriguingly, the spectrum of this source show several hints of hydrogen and helium lines, but no metal lines are detected. We theorize that this companion galaxy might be comprised mainly of Population III (PopIII) stellar remnants and potentially powers the nebular continuum emission seen in the main galaxy. These results have important implications for the presence of a potential dominant population of super-massive and PopIII stars and their consequent excess UV brightness for a significant fraction of galaxies at cosmic dawn.

**Key words.** galaxies: ISM – galaxies: starburst – galaxies: star formation - galaxies: high redshift

## 1. Introduction

The advent of the *James Webb Space Telescope* (*JWST*, Gardner et al. 2006) has provided unprecedented constraints on the rest-frame UV and optical properties of galaxies within the first billion years of cosmic time at redshifts  $z \gtrsim 5$ . One of the most significant challenges raised by *JWST* observations is the reported overabundance of UV-bright galaxies at  $z \gtrsim 10$  (e.g., Harikane et al. 2024; Whitler et al. 2025). On the one hand, this could suggest a transition in the mode of star formation to environments with enhanced star formation efficiency (Dekel et al. 2023) and stochastically varying (‘bursty’) star-formation histories (Ren et al. 2019; Mason et al. 2023; Sun et al. 2023; Gelli et al. 2024; Muñoz et al. 2026). On the other hand, it could signal variations in the mass-to-light ratio of stellar populations due to a stellar initial mass function (IMF) with a greater fraction of massive stars (‘top-heavy’ e.g., Steinhardt et al. 2023; Yung et al. 2024), or a boosting of the UV luminosity due to a stronger nebular continuum contribution than previously expected (Cameron et al. 2024; Katz et al. 2025).

The latter scenario occurs when ionizing photons are absorbed by the gas and then reprocessed into continuum emission through three different processes: free-free, free-bound, and two-photon ( $2\gamma$ , see e.g. fig. 1 of Katz et al. 2025 for a schematic). The free-bound nebular continuum, whose impact on galaxy SEDs is sometimes observed in the form of a ‘Balmer jump’

discontinuity at the wavelength of the Balmer limit, is often observed in young, low-mass, metal-poor galaxies at  $z \sim 0$  (Peimbert & Costero 1969; Guseva et al. 2006, 2007). Numerical simulations have predicted Balmer jumps to be increasingly common at high redshift (Katz et al. 2023; Wilkins et al. 2024), and a growing number of spectroscopic measurements of Balmer jumps have been made with *JWST*/NIRSpec (Roberts-Borsani et al. 2024; Cameron et al. 2024; Katz et al. 2025). Meanwhile, insights from medium-band imaging suggest that as many as  $\sim 30\%$  of galaxies may exhibit Balmer jumps by  $z \sim 6$  (Trussler et al. 2025).

In particular, Cameron et al. (2024) and Katz et al. (2025) reported several examples of so-called ‘nebular dominated galaxies’ at  $z > 4.5$ , for which both the free-bound Balmer jump in the optical and the continuum modeling suggests strong two-photon continuum. Consequently, the nebular continuum contributes  $\gtrsim 60 - 80\%$  of the rest-frame UV luminosity, with the rest originating from stellar sources. Such high nebular contribution cannot be achieved with standard stellar population models, with those authors suggesting a significant contribution from very hot stars ( $T_{\text{eff}} \gtrsim 80,000$  K), perhaps indicating exotic stellar populations and/or a very top-heavy IMF. Such a strong nebular continuum is inferred based on the combination of a clear Balmer jump, a strong UV rollover, peaking at  $1420\text{\AA}$  due to 2-photon emission, and nebular emission lines with high equivalent widths (EWs, though see e.g. Terp et al. 2024; Li et al.

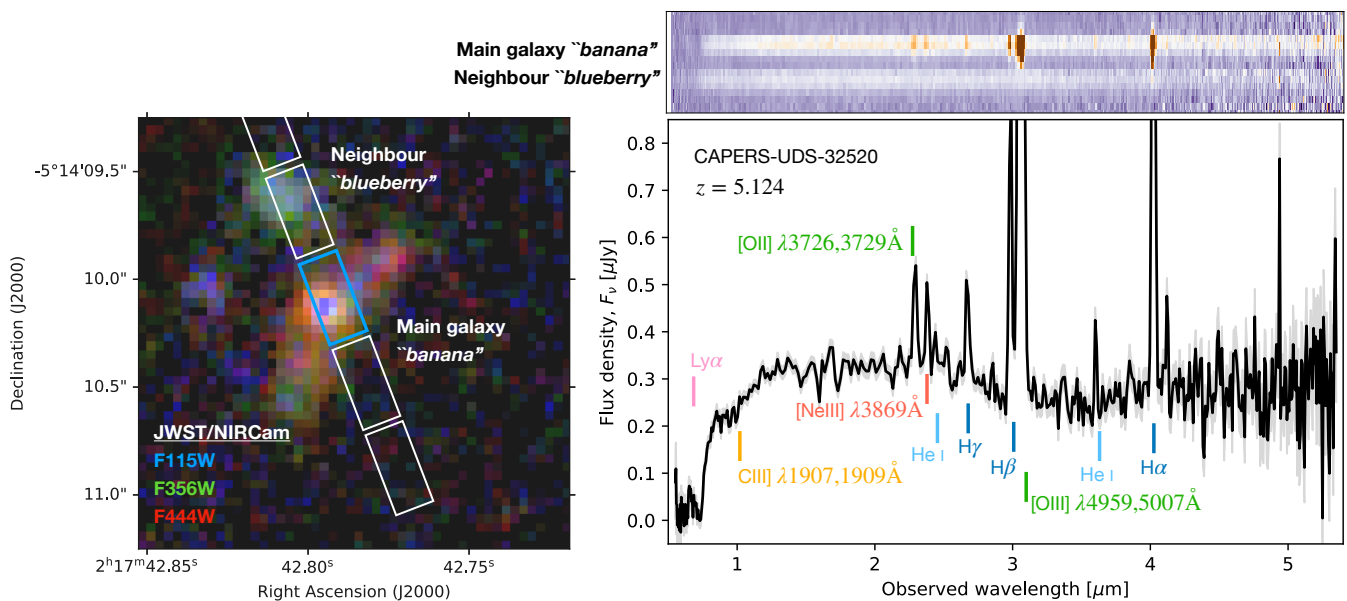


Fig. 1: (Left:) JWST/NIRCam false-color red-green-blue (RGB) thumbnail image, showing a  $2'' \times 2''$  cutouts centred on the main target (the “*banana*”) from the Primer survey (Donnan et al. 2024). (Right:) The top shows the 2D spectrum extracted from the shutter, where the bottom shows the 1D spectrum extracted using a global-average background subtraction to remove potential contamination from the nearby neighbor (the “*blueberry*”, see text for details). The most prominent emission-line features identified at the spectroscopic redshift  $z = 5.124$  are marked.

2024; Tacchella et al. 2025, for alternative interpretations). If these systems truly are powered by such extreme stellar populations, this clearly has significant implications for how the UVLF can be interpreted.

The identification of nebular-dominated galaxies and the robustness with which they can be confirmed is limited by the emergence of a large population of galaxies with strong damped Lyman- $\alpha$  absorption features ( $N_{\text{HI}} \gtrsim 10^{21} \text{ cm}^{-2}$ ) at similar redshifts (e.g., Heintz et al. 2024, 2025; Umeda et al. 2024; Hainline et al. 2024; Terp et al. 2024; Witstok et al. 2025), mimicking the predicted UV ‘rollovers’ of nebular-dominated galaxies at a given temperature. Katz et al. (2025) carried out a more systematic search for high-redshift galaxies with pronounced Balmer ‘jumps’ and provided theoretical predictions for their rest-frame UV and optical characteristics easing their identification.

Here we report the identification of a remarkable galaxy at  $z = 5.124$  observed as part of the JWST/NIRSpec Prism CANDELS-Area Prism Epoch of Reionization Survey (CAPERS; Dickinson et al. 2024), henceforth denoted as ‘CAPERS-UDS-32520’. This galaxy is characterized by a very pronounced rest-frame UV ‘rollover’ and flux excess relative to the optical continuum, exemplary of a strong Balmer jump. Notably, this galaxy does not show a Ly $\alpha$  emission feature expected for nebular-continuum-dominated galaxies and observed previously at high-redshifts (Cameron et al. 2024; Katz et al. 2025). This motivated our more detailed analysis and investigation into the underlying physical mechanisms driving the observed continuum and emission-line flux of CAPERS-UDS-32520.

We have structured the manuscript as follows: In Sect. 2, we detail the JWST imaging and spectroscopic observations of CAPERS-UDS-32520 and in Sect. 3 we present the analysis and results of the spectroscopic modeling. In Sect. 4, we examine the various likely causes for the remarkable continuum shape, and in Sect. 5 we discuss the relevance of

the potential pristine, PopIII-dominated companion galaxy detected in the image. In Sect. 6 we discuss and conclude on our work. Throughout the paper, we assume a standard  $\Lambda$ CDM concordance cosmology, with parameters adopted from Planck Collaboration et al. (2020) and applied via the AstroPy Python software (Astropy Collaboration et al. 2013) for cosmological inferences.

## 2. Observations and data processing

The spectroscopic observations of CAPERS-UDS-32520 were obtained using the NIRSpec Prism configuration of JWST with approximate resolving power  $\mathcal{R} \sim 100$  and wavelength coverage  $\lambda \sim 0.6 - 5.5 \mu\text{m}$  (Jakobsen et al. 2022) as part of the CAPERS JWST Cycle 3 program (Prog. ID: 6368, Dickinson et al. 2024). The source is located at right ascension and declination,  $\alpha, \delta(\text{J 2000}) = 02^{\text{h}}17^{\text{m}}42^{\text{s}}79, -05^{\circ}14'10''.2$  and has an absolute UV magnitude of  $M_{\text{UV}} = -20.95 \pm 0.05$  mag. The main galaxy properties are summarized in Table 1. For this work, we utilize the reduced and processed spectra of CAPERS-UDS-32520 from the DAWN JWST Archive (DJA)<sup>1</sup>. The details of these reductions are described in separate works (Heintz et al. 2025; de Graaff et al. 2025). Briefly, the raw spectroscopic data are retrieved from MAST, before they are processed with MSAExp (Brammer 2023), creating homogeneous, science-ready data products. Here we use the DJA-v4 spectra, which extends the nominal wavelength coverage of NIRSpec Prism up to  $5.5 \mu\text{m}$  and includes an improved bar shadow correction (Pollock et al. 2025). The absolute flux calibration and color corrections of this version of the spectra are typically within  $\lesssim 10\%$  of the photometrically-determined values at all wavelengths.

The final extracted 1D and 2D spectra are shown in Fig. 1. For the shown versions, we performed a global sky background

<sup>1</sup> <https://dawn-cph.github.io/dja/>

Table 1: Overview of the properties of CAPERS-UDS-32520.

R.A. (J2000)	02 <sup>h</sup> 17 <sup>m</sup> 42 <sup>s</sup> .79
Decl. (J2000)	−05°14′10″.2
$z_{\text{spec}}$	$5.1240 \pm 0.0002$
$M_{\text{UV}}$ (mag)	$-20.95 \pm 0.05$
$\beta_{\text{UV}}$	$-1.68 \pm 0.05$
$D_{\text{Ly}\alpha}$	$61.3 \pm 6.2 \text{ \AA}$
Nebular model	
$T$ (K)	$(5.3 \pm 0.2) \times 10^4$
$n_e$	$(5.4 \pm 0.8) \times 10^3$

Table 2: Detected emission-line transitions, flux densities, and rest-frame equivalent widths.

Transition	Line flux ( $\times 10^{18} \text{ erg s}^{-1} \text{ cm}^{-2}$ )	Rest-frame EW ( $\text{\AA}$ )
[O II] $\lambda\lambda 3726, 3729$	$4.2 \pm 0.5$	$35.9 \pm 4$
[Ne III] $\lambda 3869$	$2.5 \pm 0.4$	$24 \pm 5$
H $\gamma$	$2.8 \pm 0.3$	$35.14 \pm 4$
H $\beta$	$4.3 \pm 0.3$	$137.3 \pm 13$
[O III] $\lambda\lambda 4959, 5007$	$29.6 \pm 0.4$	$946 \pm 46$
He I $\lambda 5876$	$0.6 \pm 0.1$	$15 \pm 4$
H $\alpha$	$13.8 \pm 0.2$	$734 \pm 33$
He I/S I	$0.5 \pm 0.2$	$24 \pm 11$

subtraction (not included in the online DJA repository) due to the fainter blue companion galaxy seen in the left panel of Fig. 1.

The *JWST* imaging for CAPERS-UDS-32520 were obtained from the public available *JWST* Public Release IMaging for Extragalactic Research (Primer) survey (e.g., Dunlop et al. 2021; Donnan et al. 2024, GO-1837), delivering deep *JWST* NIR-Cam+MIRI imaging of the COSMOS and UDS legacy fields. For this work, we use the reduced images and photometric catalogs publicly available on DJA (see e.g., Valentino et al. 2023). The main source (the ‘banana’) is shown in Fig. 1, in close on-sky separation to a nearby companion galaxy (the ‘blueberry’) offset by  $\sim 0''.5$  or 3 kpc at the same redshift,  $z = 5.124$ .

### 3. Analysis and results

#### 3.1. The Banana and blueberry

The main galaxy CAPERS-UDS-32520 has a puzzling banana-like morphology, characterized by a bright, central ‘knot’ and more diffuse, extended emission as evidenced in Fig. 1. The origin of the extended emission is not obvious. For instance, there is no evidence of a strong foreground lensing galaxy or cluster in the images, which could otherwise cause the observed shear of the source. In the center of the knot we find a strongly dominant blue emission, here characterized by the *JWST*/NIRCam F115W filter, whereas the outskirts and the extended emission appear redder (in F356W and F444W). These gradients are commonly observed in high-redshift galaxies with *JWST* (e.g., Miller et al. 2022; Giménez-Arteaga et al. 2023), hinting at younger or less dusty stellar populations in the centers. In contrast, the companion ‘blueberry’ galaxy offset by  $\sim 0''.5$  corresponding to 3 kpc at  $z = 5.124$  shows a simple, 2D Gaussian-like profile with no hints of lensing-shear and with overall stronger continuum emission in the bluer bands. We will discuss the origin of the ‘blueberry’ companion in more detail in Sect. 5.

#### 3.2. Redshift and emission-line modeling

From the extracted *JWST*/NIRSpec Prism 1D spectrum, we identify several prominent rest-frame UV to optical nebular emission lines as marked in Fig. 1. The broad Prism wavelength coverage allows us to constrain all lines from Ly $\alpha$  at 121 nm out to 900 nm at the source redshift. We model the continuum with a simple polynomial and the detected emission lines with Gaussian line profiles, tying the redshift  $z_{\text{spec}}$  and the intrinsic full-width-half-maximum (FWHM) across the transitions. The model is convolved by the *JWST*/NIRSpec wavelength-dependent spectral resolution (Jakobsen et al. 2022), here multiplied by a factor 1.3 $\times$  from the nominal to match the observed line widths across

the spectrum (de Graaff et al. 2025). Consequently, we do not find evidence for lines intrinsically broader than the instrumental resolution ( $\gtrsim 1000 \text{ km s}^{-1}$ ). The identified lines are marked Fig. 1 and their flux densities and rest-frame equivalent widths (EWs) are reported in Table 2.

We derive a spectroscopic redshift for CAPERS-UDS-32520 of  $z_{\text{spec}} = 5.1240 \pm 0.0002$ , consistent with that reported from the automatic fitting in DJA. The galaxy is characterized by a relatively high ionization parameter, with an [O III]/[O II] line ratio of  $8.8 \pm 1.1$ . The Balmer H $\alpha$ /H $\beta$  line ratio is consistent with the intrinsic ratio expected for the Case B recombination scenario at  $T = 2 \times 10^4 \text{ K}$  (Osterbrock & Ferland 2006), implying minimal nebular dust attenuation. Using the relevant set of strong-line diagnostics from Sanders et al. (2024) based on the lines detected in the spectrum implies a relatively low metallicity, quantified in terms of the oxygen abundance as  $12 + \log(\text{O}/\text{H}) = 7.88 \pm 0.07$  corresponding to 0.15  $Z/Z_{\odot}$  solar metallicity, typical for galaxies at  $z \approx 5$  with stellar masses,  $M_{\star} \approx 10^9 M_{\odot}$  (e.g., Heintz et al. 2023; Nakajima et al. 2023).

Based on the substantial EWs of the Balmer lines, for instance H $\alpha$  is measured to have  $\text{EW}_{\text{H}\alpha} = 734 \pm 33 \text{ \AA}$ , we infer a nebular-to-stellar light fraction of  $X_{\text{neb}} \approx 10\%$  using the empirical relation described in Miranda et al. (2025). This is seemingly at odds with the prominent Balmer ‘jump’ observed in the spectrum, implying a substantially higher nebular-to-stellar continuum fraction. We will consider the scenario of strong nebular continuum further in the sections below.

#### 3.3. Rest-frame UV properties

The integrated rest-frame UV ( $\sim 1500 \text{ \AA}$ ) flux density of CAPERS-UDS-32520 implies a relatively bright continuum, with absolute UV magnitude  $M_{\text{UV}} = -20.95 \pm 0.05 \text{ mag}$ . This is among the top few percent most luminous sources at  $z > 5$  when comparing to the archival *JWST*/NIRSpec Prism ‘PRIMAL’ sample compiled by Heintz et al. (2025). Modeling the rest-frame UV spectral shape from 1250–2600  $\text{\AA}$  with a standard power-law,  $F_{\lambda} \propto \lambda^{\beta_{\text{UV}}}$ , yields a relatively ‘red’ continuum with  $\beta_{\text{UV}} = -1.68 \pm 0.05$ . This implies either a substantial amount of dust,  $A_V \sim 0.5 \text{ mag}$ , which is inconsistent with the low Balmer decrement, so more likely due to the rest-frame UV being dominated by the nebular continuum.

To quantify the physical conditions implied for the nebulae from the rest-frame UV continuum, we first consider strength of the UV rollover, quantified via the damping Ly $\alpha$  ( $D_{\text{Ly}\alpha}$ ) parameter as defined by Heintz et al. (2025). This basically measures the EW over the Ly $\alpha$  region from 1180 to 1350  $\text{\AA}$  in the rest-

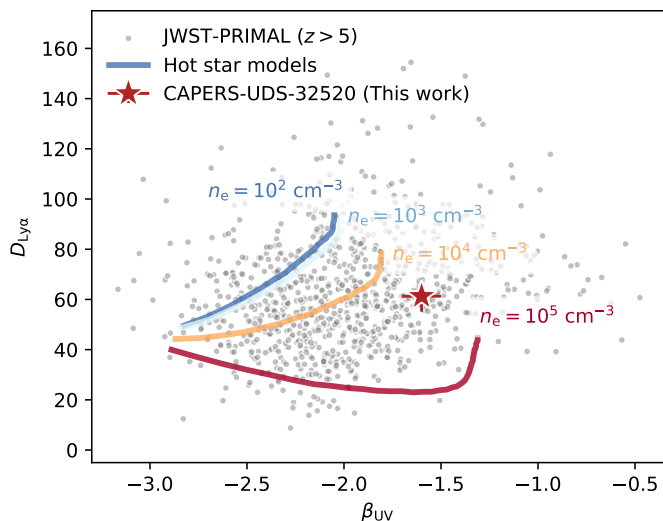


Fig. 2: Ly $\alpha$  damping parameter,  $D_{\text{Ly}\alpha}$ , as a function of the rest-frame UV spectral slope,  $\beta_{\text{UV}}$  for CAPERS-UDS-32520 (red star symbol). For comparison, the grey dots show the full PRIMAL sample at  $z > 5$  (from Heintz et al. 2025) and the colored tracks show predictions for hot metal-poor star models at various gas densities (from Katz et al. 2025).

frame. We measure  $D_{\text{Ly}\alpha} = 61.3 \pm 6.2 \text{ \AA}$ , implying either strong damped Ly $\alpha$  absorption (DLA) from H I with column density  $N_{\text{HI}} \sim 10^{23} \text{ cm}^{-2}$  or a pronounced  $2\gamma$  emission (Katz et al. 2025). These scenarios will be discussed in more detail in Sect. 4 below. As a first test, we plot the measured UV characteristics,  $\beta_{\text{UV}}$  and  $D_{\text{Ly}\alpha}$ , in Fig. 2, compared to the full JWST-PRIMAL sample (Heintz et al. 2025) and to predictions for the parameter space covered by hot metal-poor star models for a range of stellar temperatures  $T \sim 10^4 - 10^5 \text{ K}$  and densities  $n_e \sim 10^2 - 10^5 \text{ cm}^{-3}$  from Katz et al. (2025). Crucially, there is a unique combination between the  $\beta_{\text{UV}}$  and  $D_{\text{Ly}\alpha}$  for a given gas temperature and density predicted from the models. From the observed parameters for CAPERS-UDS-32520 we infer substantial gas densities  $n_e \gtrsim 10^4 \text{ cm}^{-3}$  and high temperatures,  $T \gtrsim 8 \times 10^4 \text{ K}$ , based on this model. This also implies a substantial nebular-to-stellar continuum light-ratio of  $\sim 50\%$  at  $1500 \text{ \AA}$  and  $\gtrsim 90\%$  at  $3640 \text{ \AA}$  rest-frame (Katz et al. 2025).

#### 4. The origin of the strong UV-turnover

The most prominent characteristic of this galaxy is the strong UV rollover, in combination with the red UV spectral slope and the pronounced Balmer jump. To carefully examine the origin of the broad Ly $\alpha$  damping wing and the overall spectral shape, we consider two distinct models: i) an underlying stellar continuum imprinted with a strong damped Ly $\alpha$  absorber (DLA) due to dense H I gas, see Sect. 4.1, or ii) a rest-frame UV to optical continuum dominated by  $2\gamma$  and free-bound nebular emission, see Sect. 4.2. For both scenarios, we mask out all the most prominent emission lines in the fitting, since both models are only sensitive to the continuum emission.

##### 4.1. DLA model

To model the damped Ly $\alpha$  wing, we adopt the method detailed in Heintz et al. (2024); Terp et al. (2024, Pollock et al., (subm.))

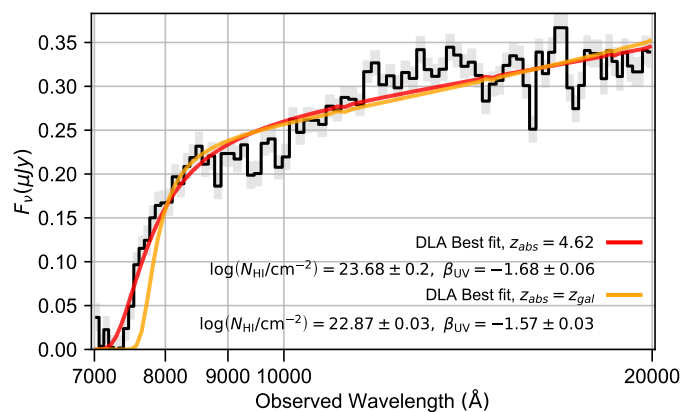


Fig. 3: JWST/NIRSpec Prism 1D spectrum, zoomed in on the rest-frame UV region. The best-fit DLA models are shown, assuming either a fixed DLA redshift to  $z_{\text{gal}}$  (yellow) or leaving the absorption redshift as a free parameter (red). The median and 16th to 84th percentiles on the output parameters from both models are summarized in the bottom-right legend.

to constrain  $N_{\text{HI}}$  in high-redshift galaxy spectra. We first assume an intrinsic rest-UV continuum described by a power law  $F_{\lambda} = F_0 \lambda^{\beta_{\text{UV}}}$ . The derived column density is typically insensitive to the exact underlying continuum, at least for strong Ly $\alpha$  damping wings (e.g., Heintz et al. 2024). The column density  $N_{\text{HI}}$  is derived by approximating the Ly $\alpha$  absorption profile as a Voigt-Hjerting function, following the prescription from Tepper Garca (2006). We also include an additional component to represent the absorption from neutral hydrogen in the IGM due to the Gunn-Peterson effect, following the method described in Miralda-Escude (1998); Totani et al. (2006). We choose a fixed neutral hydrogen fraction of  $x_{\text{HI}} = 10^{-3}$ , a conservative choice given that the universe on average is expected to be completely ionized by  $z = 5.3$  (e.g. Bosman et al. 2022). We emphasize that any damping component will be dominated by DLA gas, especially in the low resolution Prism spectrum (see e.g. Huberty et al. 2025; Heintz et al. 2025; Mason et al. 2026).

When first considering a model with fixed absorption redshift to the systemic redshift of the galaxy,  $z_{\text{abs}} = 5.124$ , we obtain a best-fit of  $N_{\text{HI}} = 10^{22.87 \pm 0.03} \text{ cm}^{-2}$  as shown by the yellow model in Figure 3. This model visually does not provide a good match to the data. Instead, leaving the absorption redshift as a free parameter, inspired by the galaxy and gas overdensity identified toward several background galaxy recovered by Terp et al. (2024); Heintz et al. (2026), we derive  $z_{\text{abs}} = 4.62$ , and  $N_{\text{HI}} = 10^{23.68 \pm 0.02} \text{ cm}^{-2}$ . Although this model is an improved visual and statistically preferred fit (red.  $\chi^2 = 2.9$  compared to red.  $\chi^2 = 5.0$ ), we caution that there is no additional evidence of a neutral gas reservoir of this magnitude or galaxy overdensities located in front of the galaxy. The extreme  $z_{\text{abs}}$  and  $N_{\text{HI}}$  derived are likely artifacts of the modeling, necessary to shift the wing and reproduce the trough seen at  $\sim 7000 \text{ \AA}$ . The highly unusual shape of the turnover is thus unlikely to be fully explained by a Ly $\alpha$  damping profile from local, dense H I gas. Finally, we note that the flux deficit seen in the spectrum from the model around  $0.9 - 1.0 \mu\text{m}$  likely arise from blends of several strong Si IV  $\lambda 1393, 1402$  and C IV  $\lambda 1548, 1550$  absorption lines in the spectrum. Alternatively, this absorption ‘bump’ would match the  $2175 \text{ \AA}$  dust bump at the suggested foreground  $z_{\text{abs}} = 4.62$ . We find this unlikely, however, given the rareness of this feature in

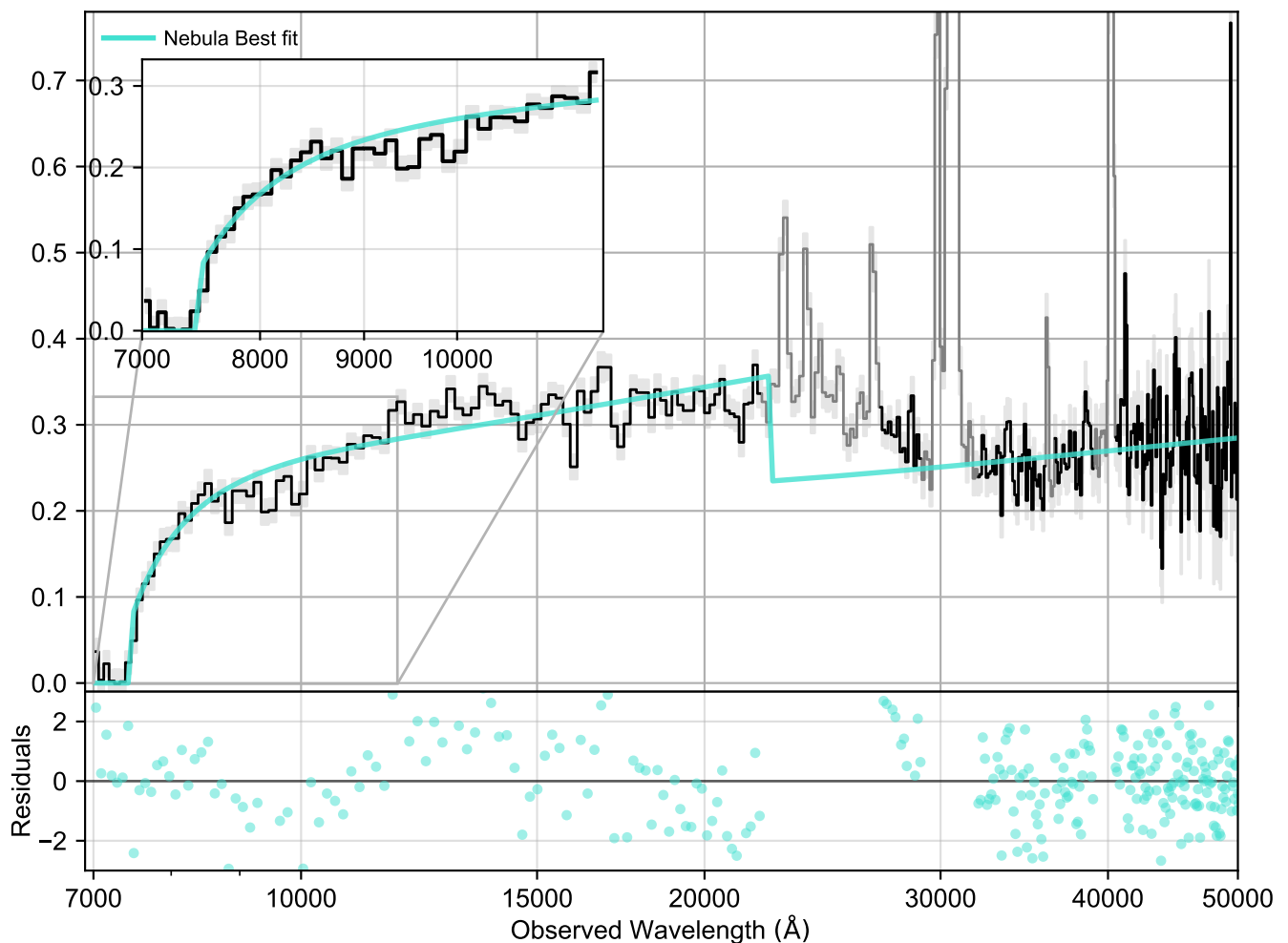


Fig. 4: *JWST*/NIRSpec Prism 1D spectrum of CAPERS-UDS-32520 (black), overlaid the best-fit nebular continuum emission model from PyNeb (cyan). The model is only constrained by the continuum, with the excluded regions shown in grey. This nebular-dominated model yields physical conditions of  $T = (5.3 \pm 0.2) \times 10^4$  K and  $n_e = (5.4 \pm 0.8) \times 10^3$  cm $^{-3}$ .

typical high-redshift galaxies (but see e.g., [Witstok et al. 2023](#); [Ormerod et al. 2025](#)).

#### 4.2. Nebular-dominated model

To test the most likely alternative scenario, we attempt to model the turnover expected from a dominant nebular continuum spectrum. To model the nebular continuum, we use the `_get_continuum1` function from PyNeb ([Luridiana et al. 2015](#)). The built-in  $T_{max}$  was increased from the nominal  $10^4$  K to  $10^5$  K to be able to fully reproduce the observed Balmer jump.

With this alternative model, we are able to model and constrain the entire continuum spectrum, from  $\sim 0.7 - 5.3\mu\text{m}$ . Our best-fit model implies an extreme nebular-dominated galaxy, with a gas temperature of  $T = (5.3 \pm 0.2) \times 10^4$  K and density  $n_e = (5.4 \pm 0.8) \times 10^3$  cm $^{-3}$ , see Fig. 4. We note that this density is lower by a factor of  $\approx 10$  to the one predicted from just the  $D_{Ly\alpha}$  and  $\beta_{UV}$  alone, suggesting that these two parameters still provide a too simple overview of the actual physical properties. The derived temperatures are substantially higher than seen in typical H II region at high redshifts though the densities match those derived from high-ion transitions (e.g., [Topping et al. 2025](#)). The strength of the Balmer jump is highly sensitive to the nebular

temperature (e.g., [Trussler et al. 2025](#)), yielding relatively tight constraints on this parameter. We include an underlying power-law in the modeling, representing the potential contribution from the stellar population in the galaxy, finding that it can only contribute up to a few percent of the observed spectrum. As a consequence, the stellar UV luminosity is of the order  $M_{UV} = -17.7$  mag, significantly less than the total observed value of  $M_{UV} = -20.95 \pm 0.05$  mag.

While this model provides a remarkable match to the data (red.  $\chi^2 = 2.3$ ) across the entire wavelength range from the rest-frame UV to optical, there is still an apparent flux deficit at  $\sim 0.9 - 1.0\mu\text{m}$ . This is expected if originating from a pseudo absorption-continuum from a blend of several high-ion absorption lines as described above. Further, the underlying continuum to the emission lines observed at  $2.3 - 2.8\mu\text{m}$  appear higher than predicted from the otherwise sharp Balmer jump transition. It is not evident what the origin of this discrepancy is, but we hypothesize a potential flux excess due to multiple blends of emission features at those wavelengths. Finally, we highlight the lack of a strong Ly $\alpha$  emission line in the spectrum, which are otherwise often observed in similar nebular-dominated galaxies (e.g., [Cameron et al. 2024](#); [Katz et al. 2025](#)). This could potentially be explained by an extra DLA component in the spectra, absorb-

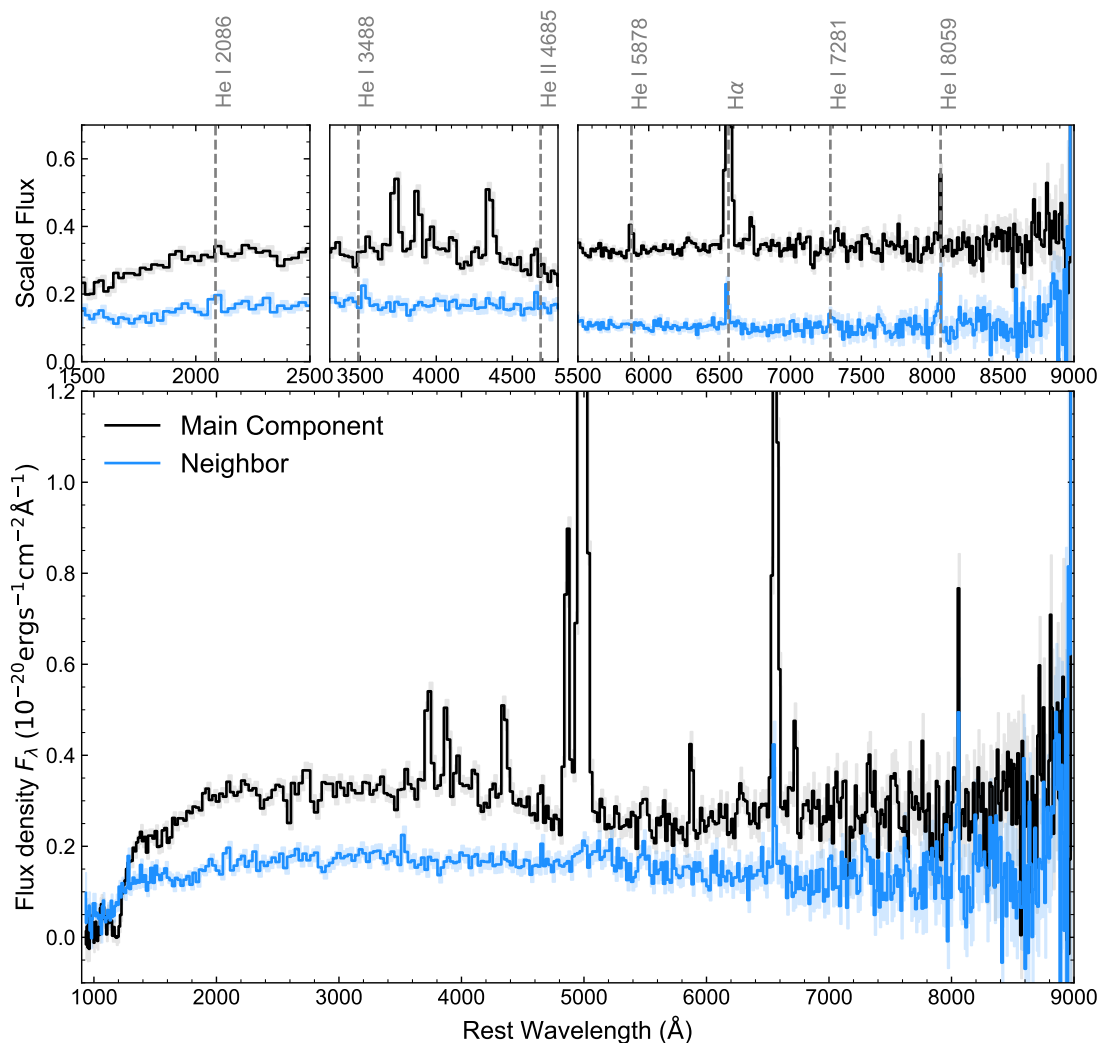


Fig. 5: JWST/Prism spectra of the main galaxy (black) and the neighbor/“blueberry” (blue). Insets show zoom-ins on potentially weak Hydrogen and Helium emission lines in both components, with a lack of any metal lines in the companion.

ing the Ly $\alpha$  photons. At the derived spectral resolution we are, however, not able to accurately constrain this, finding an approximate upper bound of  $N_{\text{HI}} \lesssim 10^{21} \text{ cm}^{-2}$  when modeled together with the nebular-continuum model.

## 5. Are PopIII stars driving the hot nebular continuum?

Under a given set of ISM conditions, the strength of the nebular continuum scales with the strength of the ionizing field powering the emission. Adopting standard stellar population models (including a Milky Way IMF), stellar populations with sufficiently young ages can power strong nebular continuum that becomes significant at rest-frame optical wavelengths, observable as a so-called Balmer jump (e.g., Guseva et al. 2007). However, these stellar populations will produce such a strong UV continuum that at  $\lambda_{\text{rest}} \approx 1500 \text{ \AA}$  the nebular continuum should be completely sub-dominant. For the nebular continuum to make a significant contribution to the emergent flux at UV wavelengths, a stellar population with ionizing photon production efficiency  $\log(\xi_{\text{ion}}) \gtrsim 25.8$  is required. Such a high value of  $\xi_{\text{ion}}$  is only physically possible with a significant presence of very hot stars with stellar temperatures  $T_{\text{eff}} \gtrsim 80,000 \text{ K}$  (Katz et al. 2025).

This particular presence of very hot stars was invoked by Cameron et al. (2024) to explain the high inferred UV nebular fraction, with those authors highlighting  $Z = 0.07 Z_{\odot}$  Wolf-Rayet stars (Todt et al. 2015), binary stripped stars (Götberg et al. 2018), or metal-free (Pop. III) stars (Zackrisson et al. 2011; Larkin et al. 2023) as possible sources of the derived hot ionizing continuum. Indeed, a nebular-dominated spectrum is a generic prediction for the emergent spectra Pop. III stellar populations (Raiter et al. 2010; Trussler et al. 2023).

The detection of oxygen and neon metal lines clearly demonstrates that the ISM of CAPERS-UDS-32520 has been enriched with metals, with a metallicity of  $12 + \log(\text{O}/\text{H}) \approx 7.8 - 8.2$  derived from measured line ratios. For the observed emission to be powered by similarly metal-enriched stars, these would be required to be in a hot, evolved phase (e.g. Wolf-Rayet stars), perhaps also with a stellar IMF skewed towards higher mass (‘top-heavy’) to further enhance the contribution of the hotter stars (e.g., Cameron et al. 2024; Cullen et al. 2025a). Alternatively, we may be witnessing metal-enriched gas being photoionized by a cluster of Pop. III stars.

With this in mind, we revisit the ‘blueberry’ companion, which serendipitously lies across the slit mask, allowing us to ex-

tract the spectrum separately to the main component, which can be compared in Figure 5. This spectrum shows clear  $H\alpha$  emission at the same redshift as CAPERS-UDS-32520. We additionally identify potential  $He I$  and  $He II$  emission lines, particularly  $He I \lambda 8059$ ,  $He I \lambda 7281$ ,  $He I \lambda 5878$  (only in main component),  $He II \lambda 4685$ ,  $He I \lambda 3488$ , and  $He I \lambda 2086$ .

A key prediction for the survival of observable Pop III galaxies to redshifts  $z \sim 5$  are potentially pristine low-mass halos, or smaller satellite galaxies (e.g. Zier et al. 2025; Yajima et al. 2023). These systems can evolve slower, and maintain pristine gas for longer; avoiding chemical enrichment and metal pollution from supernovae in the larger companion galaxy. They may also continue to accrete gas from the surrounding circumgalactic medium (CGM). Pop III remnants may therefore survive in satellite galaxies at fairly low redshifts, providing an opportunity to directly observe them with *JWST*.

Several observations of Pop III-like candidate systems have been proposed in the literature, including the  $He II \lambda 1640$  clump detected 20 kpc offset from GN-z11 (Maiolino et al. 2024), the magnified systems at  $z = 6.6$  (Vanzella et al. 2023; Nakajima et al. 2025) and  $z = 6.5$  (Fujimoto et al. 2025) with bright Balmer lines but weak [O III] metal lines, an extremely metal-poor galaxy ( $\sim 1.6\%$  solar) at  $z = 8.27$  (Cullen et al. 2025b), and a potential hybrid Pop II and Pop III system with strong  $He II$  emission but no UV metal lines (Wang et al. 2024). There is thus mounting evidence for the presence of these pristine, Pop III-like galaxies or halo systems around high-redshift galaxies uncovered by *JWST*.

## 6. Conclusions

In this work we presented the discovery and characterization of a particularly strong nebular emission dominated galaxy at  $z = 5.124$  observed as part of the CAPERS survey, called CAPERS-UDS-32520. The galaxy was identified to be likely nebular-dominated in the rest-frame UV and optical based on the prominent Balmer ‘jump’ and strong UV rollover near  $Ly\alpha$  observed in the *JWST*/NIRSpec spectrum, in addition to several strong nebular emission lines. This galaxy was particularly interesting in connection with the recent literature on similar such galaxies (e.g., Cameron et al. 2024; Katz et al. 2025), since its rest-frame UV properties indicated a particularly hot ( $T \sim 5 \times 10^4$  K) and dense ( $n_e > 10^3 \text{ cm}^{-3}$ ) gaseous region. These nebular-dominated galaxies are particularly interesting because their high gas temperatures imply exceptionally hot and potentially Pop III stars powering their emission.

We found the galaxy to show a peculiar, banana-like morphology, with a bright central ‘knot’ where the NIRSpec shutter was centered and an extended, curved emission in the north and south directions. This could hint at a potential disturbed or merger-like origin. Intriguingly, the *JWST*/NIRCam imaging from the PRIMER survey of the field revealed a ‘blue’ companion galaxy at the same redshift as the main source, offset by 3 kpc. We discussed the origin of this blue companion, the spectrum of which reveal no metal lines but several tentative hydrogen and helium lines. This indicated that the companion galaxy is likely pristine. Such pristine low-mass halos are a key prediction for the survival of observable Pop III galaxies at  $z \sim 5$ . These results thus presented an independent validation of this physical connection.

We analyzed the origin of the observed continuum and emission-line spectrum in detail, and found that it had a high ionization parameter with a [O III]/[O II] line ratio of  $8.8 \pm 1.1$ . The Balmer decrement indicated negligible amounts of dust

and based on the [O III]/ $H\beta$  ratio the galaxy is likely relatively metal-poor with  $12 + \log(O/H) = 8.0 \pm 0.2$ , typical for galaxies with stellar masses of  $\sim 10^9 M_\odot$  at  $z \approx 5$ . We found that the model with a hot and dense nebula, with gas temperature  $T = (5.3 \pm 0.2) \times 10^4$  K and  $n_e = (5.4 \pm 0.8) \times 10^3 \text{ cm}^{-3}$  was able to reproduce the entire rest-frame UV to optical continuum emission.

This model further implied that the dominant fraction ( $> 95\%$ ) of the emitted light is originating from the nebular continuum. Consequently, the stellar light of this galaxy would only have an observed UV magnitude of  $M_{UV} = -17.7$  mag, significantly less than the total observed value of  $M_{UV} = -20.95 \pm 0.05$  mag. This has strong implications for the presence of the apparent overabundant population of UV-bright galaxies at high redshifts, which might be artificially boosted if a substantial population of galaxies with strong nebular continuum exists. Gauging the impact of this population to the full underlying population of galaxies at cosmic dawn is thus essential to potentially alleviate some of the current tension in the field.

*Acknowledgements.* We express our gratitude to the investigators on the CAPERS observing programs. The work presented here would not have been possible without their major efforts in designing and obtaining the observational data included in our work here.

The data products presented herein were retrieved from the Dawn JWST Archive (DJA). DJA is an initiative of the Cosmic Dawn Center, which is funded by the Danish National Research Foundation under grant DNRF140. KEH acknowledges support from the Independent Research Fund Denmark (DRF) under grant 5251-00009B and co-funding by the European Union (ERC, HEAVYMETAL, 101071865). Views and opinions expressed are, however, those of the authors only and do not necessarily reflect those of the European Union or the European Research Council. Neither the European Union nor the granting authority can be held responsible for them. This work is based in part on observations made with the NASA/ESA/CSA James Webb Space Telescope. The data were obtained from the Mikulski Archive for Space Telescopes (MAST) at the Space Telescope Science Institute, which is operated by the Association of Universities for Research in Astronomy, Inc., under NASA contract NAS 5-03127 for JWST.

Software used in this work includes MATPLOTLIB (Hunter 2007), NUMPY (Harris et al. 2020), ASTROPY (Astropy Collaboration et al. 2013), and SCIPY (Virtanen et al. 2020).

## References

- Astropy Collaboration, Robitaille, T. P., Tollerud, E. J., et al. 2013, *A&A*, 558, A33
- Bosman, S. E. I., Davies, F. B., Becker, G. D., et al. 2022, *MNRAS*, 514, 55
- Brammer, G. 2023, *msaexp: NIRSpec analysis tools*, Zenodo
- Cameron, A. J., Katz, H., Witten, C., et al. 2024, *MNRAS*, 534, 523
- Cullen, F., Carnall, A. C., Scholte, D., et al. 2025a, *MNRAS*, 540, 2176
- Cullen, F., Carnall, A. C., Scholte, D., et al. 2025b, *MNRAS*, 540, 2176
- de Graaff, A., Brammer, G., Weibel, A., et al. 2025, *A&A*, 697, A189
- Dekel, A., Sarkar, K. C., Birnboim, Y., Mandelker, N., & Li, Z. 2023, *MNRAS*, 523, 3201
- Dickinson, M., Amorin, R., Arrabal Haro, P., et al. 2024, The CANDELS-Area Prism Epoch of Reionization Survey (CAPERS), JWST Proposal. Cycle 3, ID. #6368
- Donnan, C. T., McLure, R. J., Dunlop, J. S., et al. 2024, *MNRAS*, 533, 3222
- Dunlop, J. S., Abraham, R. G., Ashby, M. L. N., et al. 2021, PRIMER: Public Release IMaging for Extragalactic Research, JWST Proposal. Cycle 1, ID. #1837
- Fujimoto, S., Naidu, R. P., Chisholm, J., et al. 2025, *ApJ*, 989, 46
- Gardner, J. P., Mather, J. C., Clampin, M., et al. 2006, *Space Sci. Rev.*, 123, 485
- Gelli, V., Mason, C., & Hayward, C. C. 2024, *ApJ*, 975, 192
- Giménez-Arteaga, C., Oesch, P. A., Brammer, G. B., et al. 2023, *ApJ*, 948, 126
- Götberg, Y., de Mink, S. E., Groh, J. H., et al. 2018, *A&A*, 615, A78
- Guseva, N. G., Izotov, Y. I., Papaderos, P., & Fricke, K. J. 2007, *A&A*, 464, 885
- Guseva, N. G., Izotov, Y. I., & Thuan, T. X. 2006, *ApJ*, 644, 890
- Hainline, K. N., D’Eugenio, F., Jakobsen, P., et al. 2024, *ApJ*, 976, 160
- Harikane, Y., Nakajima, K., Ouchi, M., et al. 2024, *ApJ*, 960, 56
- Harris, C. R., Millman, K. J., van der Walt, S. J., et al. 2020, *Nature*, 585, 357

- Heintz, K. E., Bennett, J. S., Oesch, P. A., et al. 2026, *Nature Astronomy*
- Heintz, K. E., Brammer, G. B., Giménez-Arteaga, C., et al. 2023, *Nature Astronomy*, 7, 1517
- Heintz, K. E., Brammer, G. B., Watson, D., et al. 2025, *A&A*, 693, A60
- Heintz, K. E., Watson, D., Brammer, G., et al. 2024, *Science*, 384, 890
- Huberty, M., Scarlata, C., Hayes, M. J., & Gazagnes, S. 2025, *ApJ*, 987, 82
- Hunter, J. D. 2007, *Computing in Science and Engineering*, 9, 90
- Jakobsen, P., Ferruit, P., Alves de Oliveira, C., et al. 2022, *A&A*, 661, A80
- Katz, H., Cameron, A. J., Saxena, A., et al. 2025, *The Open Journal of Astrophysics*, 8, 104
- Katz, H., Rosdahl, J., Kimm, T., et al. 2023, arXiv e-prints, arXiv:2309.03269
- Larkin, M. M., Gerasimov, R., & Burgasser, A. J. 2023, *AJ*, 165, 2
- Li, Y., Leja, J., Johnson, B. D., Tacchella, S., & Naidu, R. P. 2024, *ApJ*, 969, L5
- Luridiana, V., Morisset, C., & Shaw, R. A. 2015, *A&A*, 573, A42
- Maiolino, R., Übler, H., Perna, M., et al. 2024, *A&A*, 687, A67
- Mason, C. A., Chen, Z., Stark, D. P., et al. 2026, *A&A*, 705, A114
- Mason, C. A., Trenti, M., & Treu, T. 2023, *MNRAS*, 521, 497
- Miller, T. B., Whitaker, K. E., Nelson, E. J., et al. 2022, *ApJ*, 941, L37
- Miralda-Escudé, J. 1998, *ApJ*, 501, 15
- Miranda, H., Pappalardo, C., Afonso, J., et al. 2025, *A&A*, 694, A102
- Muñoz, J. B., Chisholm, J., Sun, G., et al. 2026, arXiv e-prints, arXiv:2601.07912
- Nakajima, K., Ouchi, M., Harikane, Y., et al. 2025, arXiv e-prints, arXiv:2506.11846
- Nakajima, K., Ouchi, M., Isobe, Y., et al. 2023, *ApJS*, 269, 33
- Ormerod, K., Witstok, J., Smit, R., et al. 2025, *MNRAS*, 542, 1136
- Osterbrock, D. E. & Ferland, G. J. 2006, *Astrophysics of gaseous nebulae and active galactic nuclei*
- Peimbert, M. & Costero, R. 1969, *Boletín de los Observatorios Tonantzintla y Tacubaya*, 5, 3
- Planck Collaboration, Aghanim, N., Akrami, Y., et al. 2020, *A&A*, 641, A6
- Pollock, C. L., Gottumukkala, R., Heintz, K. E., et al. 2025, arXiv e-prints, arXiv:2506.15779
- Raiter, A., Schaerer, D., & Fosbury, R. A. E. 2010, *A&A*, 523, A64
- Ren, K., Trenti, M., & Mason, C. A. 2019, *ApJ*, 878, 114
- Roberts-Borsani, G., Treu, T., Shapley, A., et al. 2024, *ApJ*, 976, 193
- Sanders, R. L., Shapley, A. E., Topping, M. W., Reddy, N. A., & Brammer, G. B. 2024, *ApJ*, 962, 24
- Steinhardt, C. L., Kokorev, V., Rusakov, V., Garcia, E., & Sneppen, A. 2023, *ApJ*, 951, L40
- Sun, G., Faucher-Giguère, C.-A., Hayward, C. C., et al. 2023, *ApJ*, 955, L35
- Tacchella, S., McClymont, W., Scholtz, J., et al. 2025, *MNRAS*, 540, 851
- Tepper García, T. 2006, *Monthly Notices of the Royal Astronomical Society*, 369, 2025–2035
- Terp, C., Heintz, K. E., Watson, D., et al. 2024, *A&A*, 690, A70
- Todt, H., Sander, A., Hainich, R., et al. 2015, *A&A*, 579, A75
- Topping, M. W., Sanders, R. L., Shapley, A. E., et al. 2025, *MNRAS*, 541, 1707
- Totani, T., Kawai, N., Kosugi, G., et al. 2006, *PASJ*, 58, 485
- Trussler, J. A. A., Cameron, A. J., Eisenstein, D. J., et al. 2025, arXiv e-prints, arXiv:2510.12622
- Trussler, J. A. A., Conselice, C. J., Adams, N. J., et al. 2023, *MNRAS*, 525, 5328
- Umeda, H., Ouchi, M., Nakajima, K., et al. 2024, *ApJ*, 971, 124
- Valentino, F., Brammer, G., Gould, K. M. L., et al. 2023, *ApJ*, 947, 20
- Vanzella, E., Loiacono, F., Bergamini, P., et al. 2023, *A&A*, 678, A173
- Virtanen, P., Gommers, R., Oliphant, T. E., et al. 2020, *Nature Methods*, 17, 261
- Wang, X., Cheng, C., Ge, J., et al. 2024, *ApJ*, 967, L42
- Whitler, L., Stark, D. P., Topping, M. W., et al. 2025, *ApJ*, 992, 63
- Wilkins, S. M., Lovell, C. C., Irodotou, D., et al. 2024, *MNRAS*, 527, 7965
- Witstok, J., Jakobsen, P., Maiolino, R., et al. 2025, *Nature*, 639, 897
- Witstok, J., Shivaiei, I., Smit, R., et al. 2023, *Nature*, 621, 267
- Yajima, H., Abe, M., Fukushima, H., et al. 2023, *MNRAS*, 525, 4832
- Yung, L. Y. A., Somerville, R. S., Finkelstein, S. L., Wilkins, S. M., & Gardner, J. P. 2024, *MNRAS*, 527, 5929
- Zackrisson, E., Rydberg, C.-E., Schaerer, D., Östlin, G., & Tuli, M. 2011, *ApJ*, 740, 13
- Zier, O., Kannan, R., Smith, A., et al. 2025, *MNRAS*, 544, 410

**Appendix A: Posterior results on the nebular fitting**

Here is provided the full corner plot of the nebula model described in Sect. 4.2.

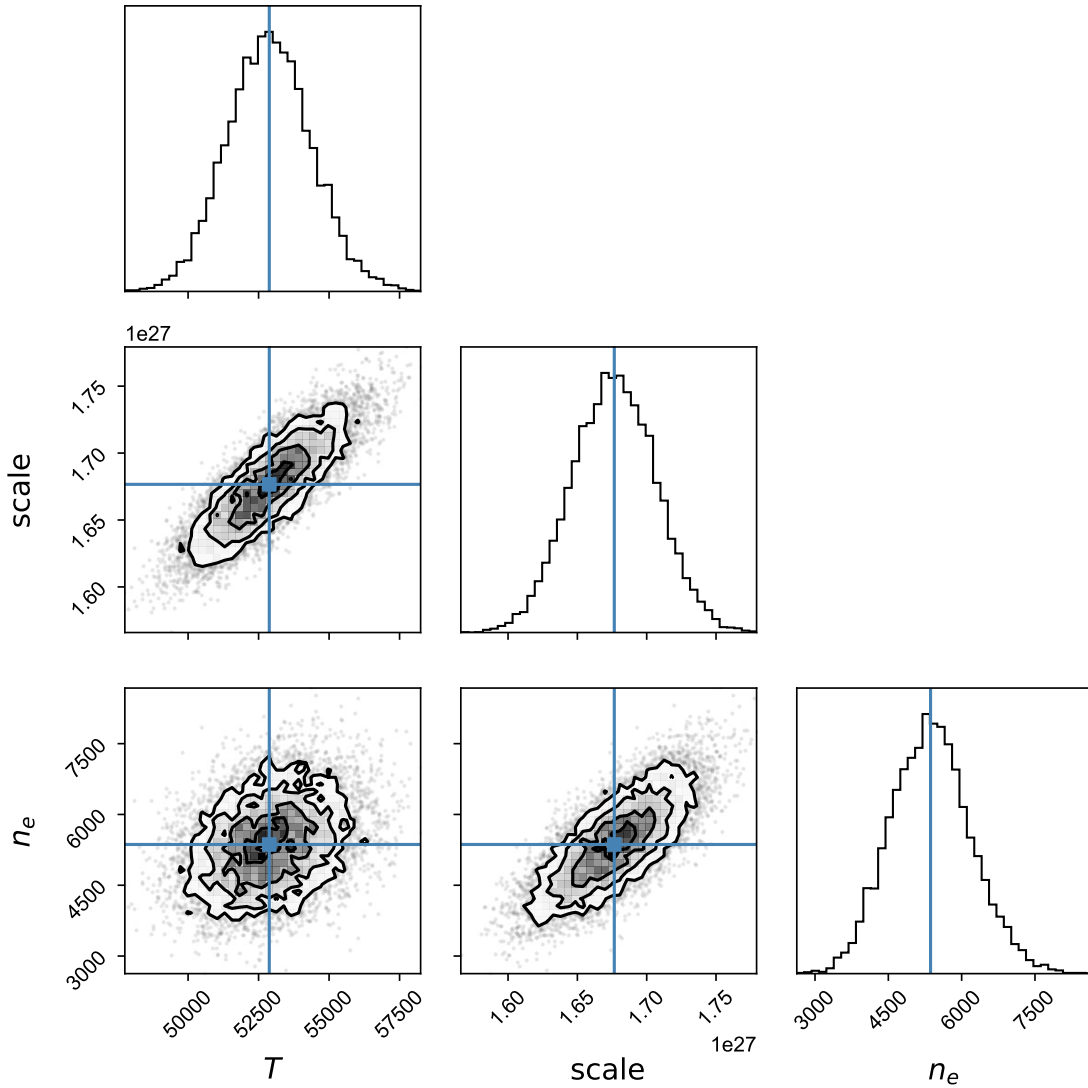


Fig. A.1: The posterior plot for the nebula model. All posterior distributions are clearly gaussian and the best fit parameters are well defined within the parameter space.